ELSEVIER

Journal of Alloys and Compounds 303–304 (2000) 465–471

Journal of ALLOYS AND COMPOUNDS

www.elsevier.com/locate/jallcom

# Hydrothermal synthesis and properties of $Ce_{1-x}Eu_xO_{2-\delta}$ solid solutions☆

P. Shuk[a], M. Greenblatt[a,*], M. Croft[b]

[a]*Department of Chemistry, Rutgers, The State University of New Jersey, 610 Taylor Rd, Piscataway, NJ 08854-8087, USA*
[b]*Department of Physics and Astronomy, Rutgers, The State University of New Jersey, Piscataway, NJ 08854-8019, USA*

**Abstract**

The structure, thermal expansion coefficients and ionic and electronic conductivities of $Ce_{1-x}Eu_xO_{2-\delta}$ ($x = 0$–$0.50$) solid solutions, prepared hydrothermally for the first time, were investigated. The uniformly small particle size (40–55 nm) of the hydrothermally prepared materials allows sintering of the samples into highly dense ceramic pellets at 1300–1400°C, a significantly lower temperature than 1600–1650°C, which is required for samples prepared by solid-state techniques. X-ray absorption spectroscopy (XAS) was used to establish the pure $Eu^{3+}$ character of the europium ions; XAS also reflects local disorder effects. The highest conductivity was found for $Ce_{0.85}Eu_{0.15}O_{1.925-\delta}$ ($\sigma_{700°C} = 2.6 \times 10^{-2}$ S/cm, $E_a = 0.66$ eV) with predominantly oxide-ion mobility. 

*Keywords:* Hydrothermal synthesis; Ionic conductivity; Electronic conductivity; Thermal expansion coefficients

## 1. Introduction

The solid electrolyte is a key component of solid-state electrochemical devices, which are increasingly important for applications in energy conversion, chemical processing, sensing and combustion control [1–3]. High oxide-ion conducting solid electrolytes based on $ZrO_2$ (zirconia) have been extensively investigated and reviewed in the past as well as successfully applied in various electrochemical devices [4–8]. Although stabilized zirconia is considered to be the most reliable solid electrolyte so far, many studies have been made on other solid electrolytes as alternatives to zirconia, e.g. $Bi_2O_3$- [9–11] and $CeO_2$-based [12] materials to increase the efficiency of the electrochemical device and decrease the application temperature. In the past several years, $CeO_2$-based materials have been intensely investigated as catalysts, structural and electronic promoters of heterogeneous catalytic reactions and oxide-ion conducting solid electrolytes in electrochemical cells [12–14]. For the last of these applications relatively high ionic conductivity of the solid electrolyte is required for device performance. The oxygen vacancy ($V_O^{\cdot\cdot}$) concentration, and concomitant oxide-ion conductivity, in cerium oxide can be increased by the substitution of a lower-valent metal ion (e.g., $M^{3+}$) for the cerium. In the past, many investigations have been carried out on various aspects of ceria solid electrolytes mostly prepared by conventional ceramic methods [12]. However, the preparation temperature or time needed to obtain a homogeneous solid solution depends significantly on the particle size of the starting materials. Yttrium- and samarium-doped ceria solid electrolytes have been successfully prepared by the hydrothermal method, providing low-temperature preparation and morphological control of ultrafine particles of uniform crystallite dimension [15,16]. Recently, we have shown that solid solutions of $Ce_{1-x}Sm_xO_{2-x/2}$ and $Ce_xCa_xO_{2-x}$ can be hydrothermally prepared in a wide substitution range of Sm or Ca [17].

While past efforts in solid-state ionics focused on expanding the electrolytic domain of oxide-ion conducting solid electrolytes for application in solid oxide fuel cells (SOFC) or sensors, more recently efforts have begun to introduce enhanced electronic conduction in high ionically conductive matrices to develop mixed conductors for oxygen membrane application [18]. For this application, equally high electronic and ionic conductivities are required to achieve maximum oxygen flux through the membrane needed for oxygen separation [18,19]. The flux of oxygen at a given total conductivity is maximum when the ionic and electronic conductivities are equal.

Teraoka et al. [20] were the first to report, in addition to very high electronic conductivity, high oxide-ion conductivity and associated high oxygen permeability in perovskite-type materials. Presently, extensive research is

☆In memory of Professor Wolfgang Göpel.

*Corresponding author. Fax: +1-732-445-5312.
*E-mail address:* martha@rutchem.rutgers.edu (M. Greenblatt)

0925-8388/00/$ – see front matter 
PII: S0925-8388(00)00627-7

being conducted on acceptor-doped perovskite oxides $Ln_{1-x}A_xCo_{1-y}B_yO_{3-\delta}$ (A=Ca, Sr, Ba; B=Fe, Cu, Ni, Mn) [18]. The structural and chemical integrity of the cobaltites as well as their very high thermal expansion coefficients ($>20\times10^{-6}$ $K^{-1}$) are limiting factors for their application as oxygen membranes.

More reliable oxygen membranes may be developed based on fluorite-type oxide-ion conducting solid electrolytes, which are more stable and have considerably smaller thermal expansion coefficients ($\sim10^{-5}$ $K^{-1}$), if equally high electronic conductivity can be introduced into the fluorite matrix. Recently, we have shown that the oxygen permeability, $J(O_2)$, of Pr- [21] or Tb-substituted [22] ceria [e.g., $J(O_2)=1.9\times10^{-10}$ mol/s-cm for $Ce_{0.70}Pr_{0.30}O_{1.85+\delta}$ at 700°C] is close to the oxygen permeability value of the mixed conductors based on the best conductive bismuth oxide solid electrolytes [18]. Another rare earth element Eu, like Pr or Tb, is known to have mixed valency ($Eu^{3+}/Eu^{2+}$).

In this paper we present a systematic study of the structure, ionic and electronic conductivities and thermophysical properties of europium-substituted ceria solid solutions, $Ce_{1-x}Eu_xO_{2-\delta}$, prepared for the first time hydrothermally.

## 2. Experimental

Solid solutions of $Ce_{1-x}Eu_xO_{2-\delta}$ ($x=0$–$0.50$) were synthesized by the hydrothermal method as previously reported for Tb-doped ceria [21]. The appropriate quantities of cerium (III) nitrate hexahydrate ($Ce(NO_3)_3\cdot6H_2O$, 99.9% Aldrich), and europium (III) nitrate pentahydrate ($Eu(NO_3)_3\cdot5H_2O$, 99.9% Alfa) were dissolved separately in water, mixed and coprecipitated with ammonium hydroxide at pH 10. The precipitated gels were sealed in Teflon-lined steel autoclaves and hydrothermally treated at 260°C for 10 h (Fig. 1). The autoclaves were quenched at 260°C and the crystallized powder products were repeatedly washed with deionized water and dried in air at room temperature.

The room/high temperature powder X-ray diffraction patterns (PXD) of the ultrafine powders were obtained with a SCINTAG PAD V diffractometer equipped without/with a high temperature attachment with monochromatized Cu Kα radiation at a $2\theta$ scan of 0.5°/min. Cell parameters were calculated by fitting the observed reflections with a least-squares program. The reflection from the (422) plane was used for the determination of average crystallite size. The average crystallite size, $D$, of the hydrothermally prepared powders was calculated from the Scherrer formula:

$$D=\frac{0.9\lambda}{\beta\cos\theta} \quad (1)$$

where $\lambda$ is the wavelength of the X-rays, $\theta$ is the diffraction angle, $\beta=\sqrt{(\beta_m^2-\beta_s^2)}$ is the corrected halfwidth of the observed halfwidth, $\beta_m$, of the (422) reflection in samples of $Ce_{1-x}Eu_xO_{2-\delta}$, and $\beta_s$ is the halfwidth of the (422) reflection in a standard sample of $CeO_2$ ($D\sim100$ nm). Differential thermal analysis (DTA) and thermogravimetric analysis (TGA) measurements were carried out in the temperature range 25–750°C with a TA Instruments DSC 2910 and TGA 2050 with a heating and cooling rate of 1°C/min.

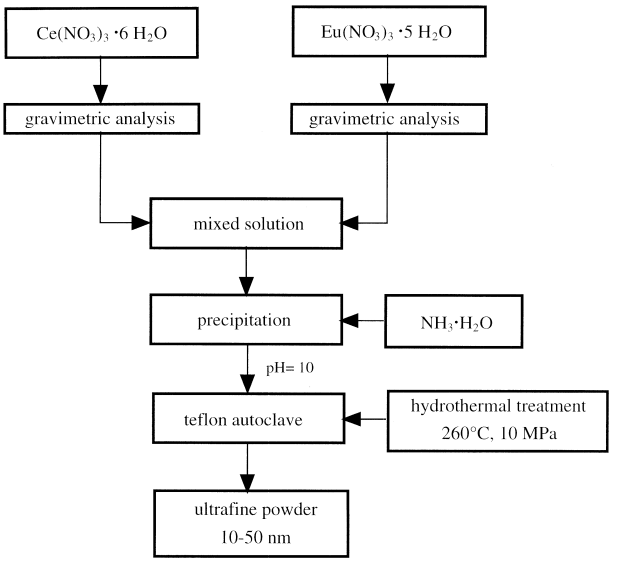


Fig. 1. Flow diagram of the hydrothermal synthesis.

The powder samples were pelletized and sintered at 1300–1400°C for 4 h with a programmed heating and cooling rate of 5°C/min. The sintered samples were over 95–97% of the theoretical density in all cases. The microstructure of sintered samples was studied with an atomic force microscope (AFM, QScope Model 250, Quesant Instrument Corp., CA). The ionic conductivity measurements were performed on sintered ceramic disk pellets by the complex impedance method at frequencies ranging from 0.1 Hz to 65 kHz (Solartron 1280 Frequency Response Analyser). Electronic conductivities were also measured by the four-point DC method (to check the contribution of electrons to the total conductivity) on sintered rectangular samples in air on heating and cooling in the temperature range 300–700°C. Silver paste was painted onto two faces of the samples, using GC Electronics paste. The samples were then dried and fired at 650°C. In order to determine the oxide-ion transference numbers, the EMF of the following oxygen concentration cell was measured:

$$p(O_2)^a, O_2, Ag|Ce_{1-x}Eu_xO_{2-\delta}\ \text{sample}|Ag, O_2, p(O_2)^c \quad (2)$$

If the conduction in ceria solid solutions is predominantly ionic, the theoretical EMF ($E_{th}$) is given by the Nernst equation:

$$E_{th} = \frac{RT}{4F} \ln \frac{p(O_2)^c}{p(O_2)^a} \quad (3)$$

where $R$, $T$, and $F$ are the gas constant, the temperature and the Faraday constant, respectively, and $p(O_2)^a = 1.01 \times 10^5$ Pa and $p(O_2)^c = 0.21 \times 10^5$ Pa are oxygen partial pressures at the anode (pure oxygen) and cathode (air), respectively. If the specimen has some electronic conduction, the measured EMF ($E$) will be lower than $E_{th}$ because of the discharge of the electrochemical cell due to the electronic conduction. If the electrodes are sufficiently reversible the oxide-ion transference numbers, $t_i$, can be calculated as follows:

$$t_i = \frac{\sigma_i}{\sigma_i + \sigma_e} = \frac{E}{E_{th}} \quad (4)$$

where $\sigma_i$ and $\sigma_e$ are the ionic and electronic conductivities, respectively.

The Eu $L_3$-edge X-ray absorption spectroscopy measurements were performed on beam line X-18B at the Brookhaven National Synchrotron Light Source using a channel cut Si(111) monochromator. Fluorescence mode and transmission mode measurements were made and checked for consistency. All spectra were normalized to unity in the absorption coefficient from well below to well above the edge.

## 3. Results and discussion

The PXD data in Fig. 2 show that $Ce_{1-x}Eu_xO_{2-\delta}$, prepared by hydrothermal synthesis for the first time, forms solid solutions with the fluorite structure in the Eu substitution range $x = 0$–$0.25$. At higher substitution the separation of a second phase based on $Eu_2O_3$ is observed. The fluorite-phase evolution of $Ce_{0.75}Eu_{0.25}O_{1.875-\delta}$ in the hydrothermal process as a function of heat-treatment time at 260°C was examined by PXD. After 20 min heating, the precipitated product is a fine crystalline powder (~25 nm average particle size) of cerium/europium solid solution and europium oxide (Fig. 3). Further hydrothermal heat treatment increases the crystallinity of the powder: for example, 34 nm in 40 min, 45 nm in 60 min, and ~50 nm in 12 h, and leads to a single phase solid solution.

The unit cell parameter $a$ increases with increasing Eu content (Fig. 4), in good agreement with effective ionic radii considerations ($r_{Ce^{4+}} = 0.111$ nm, $r_{Eu^{3+}} = 0.1206$ nm [23]). The solubility limit of $Eu_2O_3$ in $CeO_2$ was found to be ~25%.

The average crystallite size, $D$, of europium-substituted ceria powders, calculated by the Scherrer formula from the PXD data, were between 40 and 55 nm (Table 1). The fine, substituted ceria powders were sintered at 1300–1400°C into pellets and rectangular samples with apparent densities over 95–97% of the theoretical value. In contrast, ceria solid electrolytes prepared by conventional ceramic techniques require over 1600°C for sintering.

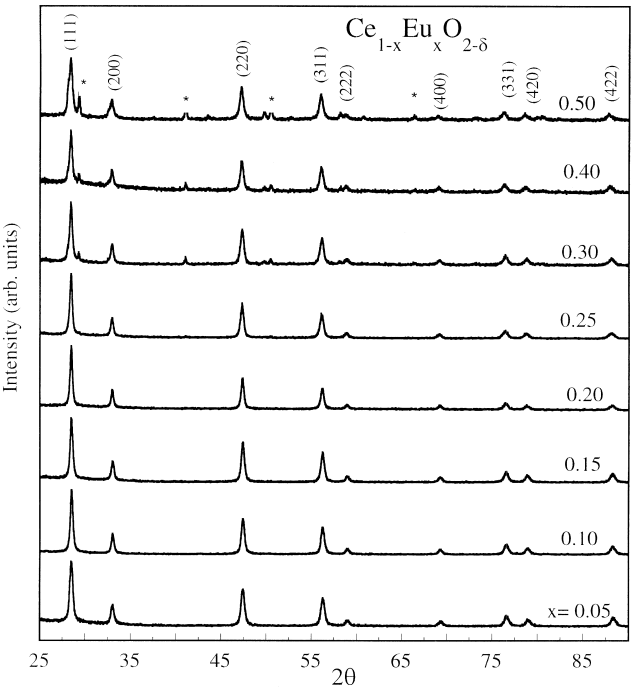


Fig. 2. Powder X-ray diffraction patterns of $Ce_{1-x}Eu_xO_{2-\delta}$ solid solutions quenched at 260°C.

Temperature dependent X-ray diffraction measurements show no transformation of the fluorite structure nor phase

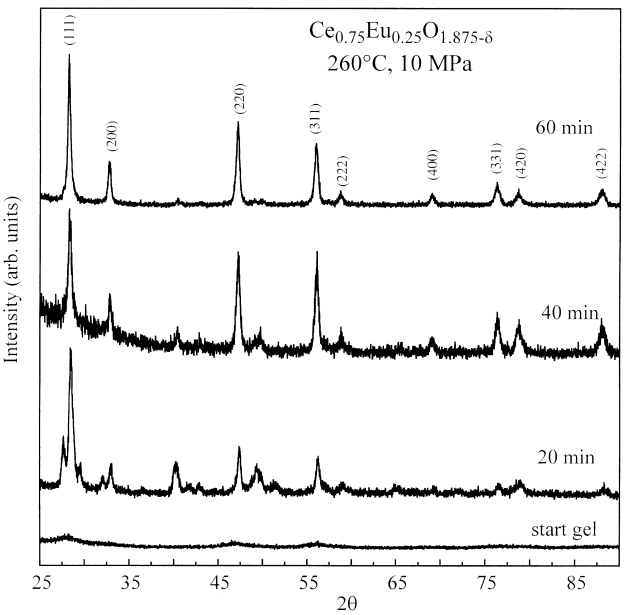


Fig. 3. Evolution of the powder X-ray diffraction patterns as a function of time of a hydrothermally prepared $Ce_{0.75}Eu_{0.25}O_{1.875-\delta}$ solid solution quenched at 260°C.

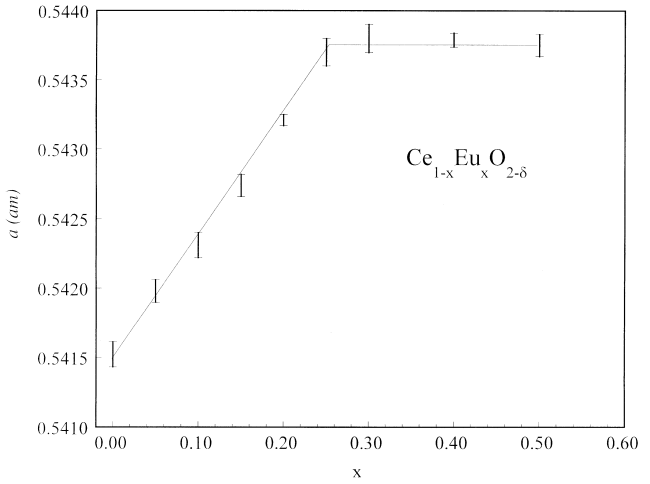


Fig. 4. Lattice constants of $Ce_{1-x}Eu_xO_{2-\delta}$ solid solutions as a function of $x$.

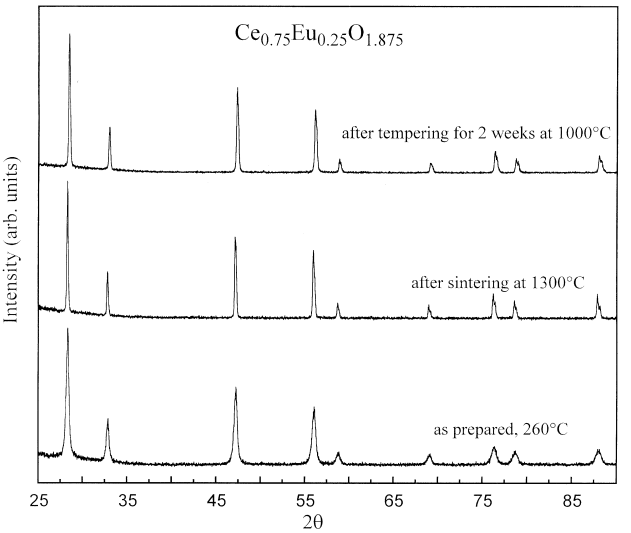


Fig. 5. Powder X-ray diffraction patterns of $Ce_{0.75}Eu_{0.25}O_{1.875-\delta}$ after treatment at different temperatures.

separation of $Eu_2O_3$ in $Ce_{0.75}Eu_{0.25}O_{1.875-\delta}$ after sintering at 1300°C for 4 h or after annealing at 1000°C for 2 weeks (Fig. 5). The crystallite size increases from 40 nm after hydrothermal preparation at 260°C to ~170 nm after annealing for 2 weeks at 1000°C and to ~260 nm after sintering at 1300°C. The lattice constant, $a$, increases linearly with temperature; the thermal expansion coefficients determined from these data are $11.8\times10^{-6}$ $K^{-1}$ for $CeO_2$ and slightly increase with increasing Eu content to $14.0\times10^{-6}$ $K^{-1}$ for $Ce_{0.75}Eu_{0.25}O_{1.875-\delta}$.

In Fig. 6 the AFM topographic image of a $Ce_{0.75}Eu_{0.25}O_{1.875-\delta}$ sample sintered at 1300°C indicates relatively small particles of uniform size, ~0.5–1 μm, and a very dense microstructure. As expected, these particles are considerably larger than those of the ''as-prepared'' powder (~55 nm).

Pure ceria oxide is basically a poor oxide-ion conductor ($\sigma_{700°C} = 1.9\times10^{-5}$ S/cm). The ionic conductivities are significantly enhanced in $Ce_{1-x}Eu_xO_{2-\delta}$ solid electrolytes (Fig. 7) by the substitution of $Ce^{4+}$ by $Eu^{3+}$, leading to an increase of the oxygen vacancies, $V_O^{\cdot\cdot}$:

$$2CeO_2 \overset{Eu_2O_3}{\rightarrow} 2Eu'_{Ce} + 3O_O^x + V_O^{\cdot\cdot} + \tfrac{1}{2}O_2 \quad (5)$$

The ionic conductivity of $Ce_{1-x}Eu_xO_{2-x/2}$ increases systematically with increasing europium substitution and reaches a maximum at $x = 0.15$ (Figs. 7 and 8). As noted before [17,22], the decrease in the ionic conductivity for higher $x$ (here for $x > 0.15$) is ascribed to defect associations of the type $\{Eu'_{Ce}\,V_O^{\cdot\cdot}\}$ at higher concentrations of $V_O^{\cdot\cdot}$. At higher substitution ($x > 0.25$) a separation of the second, less conductive phase, $Eu_2O_3$, leads to a decrease in the conductivity. A knee seen at ~500°C in the conductivity plots of the samples with $x > 0.25$ is attributed to a change in the mechanism of conductivity. Above 500°C the oxide-ion conductivity of $Ce_{1-x}Eu_xO_{2-\delta}$ ($x$ = 0.30–0.50) dominates over the electronic conductivity of $Eu_2O_3$. The ionic transference number measurements with a concentration electrochemical cell (2) have shown that the conductivity of the $Ce_{1-x}Eu_xO_{2-\delta}$ fluorite phase is predominantly ionic ($t_i > 0.99$). The activation enthalpy for

Table 1
Lattice parameters, crystallite sizes and electrical properties of $Ce_{1-x}Eu_xO_{2-\delta}$ solid solutions

| Composition | Lattice parameter $a$ (nm) | Average crystallite size $D$ (nm) | Conductivity $\sigma_{700°C}$ (S/cm) (±5%) | Activation energy $E_a$ (eV) (±0.05) |
|---|---|---|---|---|
| $x = 0$ | 0.54152(9) | 40 | $1.9\times10^{-5}$ | 1.03 |
| 0.05 | 0.54198(8) | 40 | $1.4\times10^{-3}$ | 0.73 |
| 0.10 | 0.54231(9) | 50 | $1.8\times10^{-2}$ | 0.78 |
| 0.15 | 0.54274(8) | 50 | $2.6\times10^{-2}$ | 0.66 |
| 0.20 | 0.54321(4) | 55 | $2.5\times10^{-2}$ | 0.77 |
| 0.25 | 0.5437(1) | 55 | $2.0\times10^{-2}$ | 0.79 |
| 0.30 | 0.5438(1) | 45 | $1.8\times10^{-2}$ | 0.84 |
| 0.40 | 0.54379(5) | 50 | $4.0\times10^{-3}$ | 1.1 (>500°C)<br>0.70 (<500°C) |
| 0.50 | 0.54375(8) | 40 | $5.8\times10^{-4}$ | 1.2 (>500°C)<br>0.71 (<500°C) |

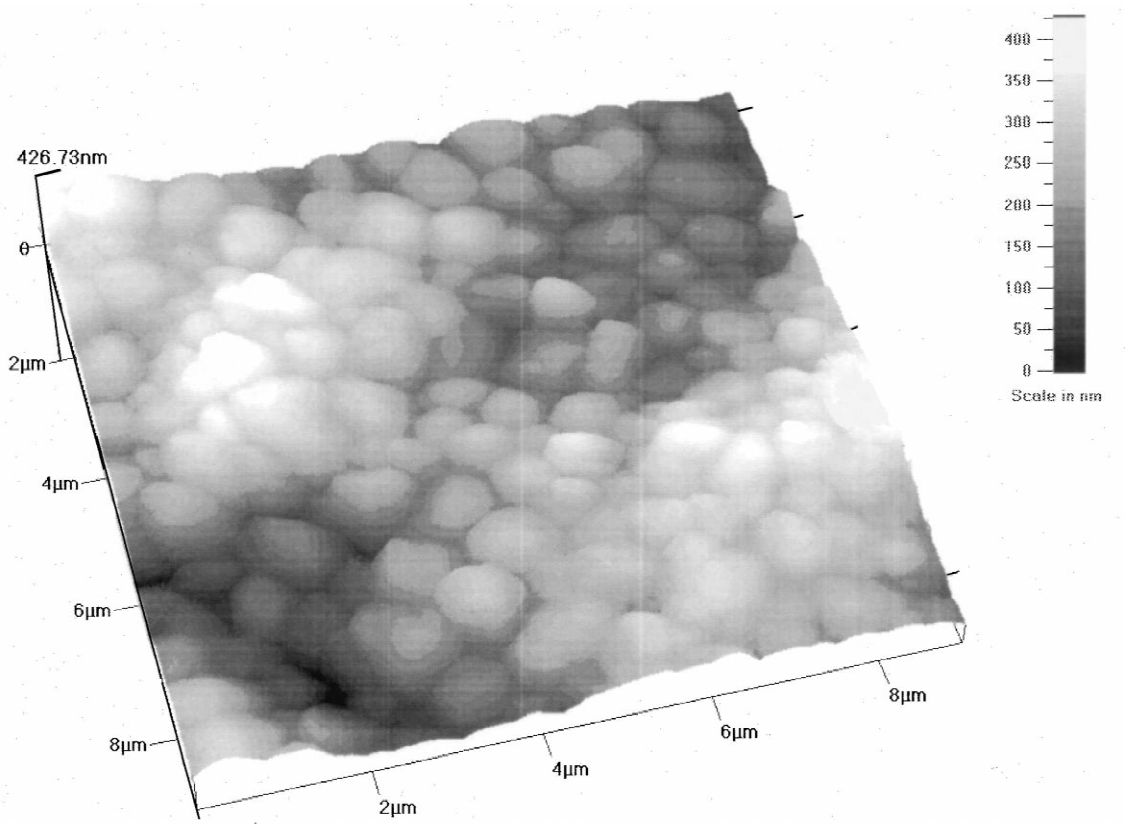


Fig. 6. In-situ AFM topographic image of a sintered (1300°C) $Ce_{0.26}Eu_{0.25}O_{1.875-\delta}$ sample.

conductivity first decreases with increasing Eu substitution (Table 1) due to the weaker Eu(III)–O bond compared to that of Ce(IV)–O, and reaches the minimum at $x = 0.15$ (0.66 eV). At $x > 0.15$ substitutions the activation enthalpy increases, because of the increasing contribution of the association enthalpy ($\Delta H = \Delta H_m + \Delta H_a$, $\Delta H_m$ is the migration enthalpy for oxide ions, $\Delta H_a$ is the enthalpy for the defect associates, $\{Eu'_{Ce}\ V_O^{\cdot\cdot}\}$).

We have performed Eu $L_3$ X-ray absorption spectroscopy (XAS) studies of $Ce_{1-x}Eu_xO_{2-\delta}$ materials. In Fig. 9, a comparison of the observed intense WL feature of $Ce_{0.75}Eu_{0.25}O_{2-\delta}$ (due to transitions into the Eu 5d final

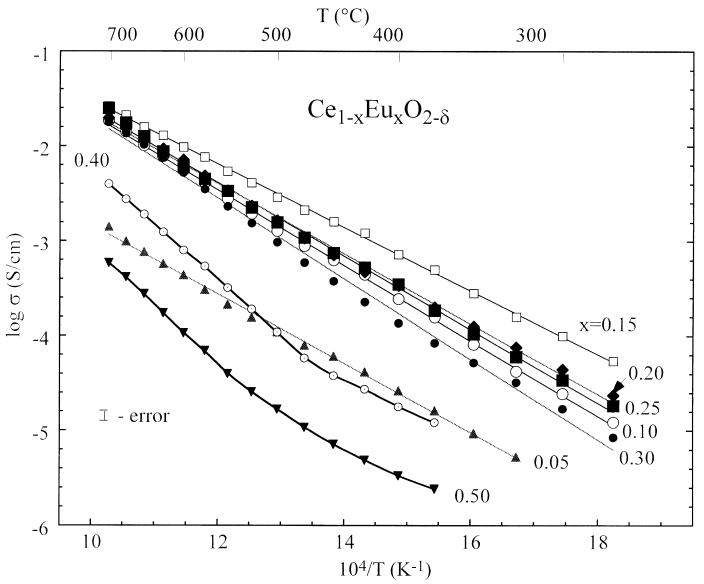


Fig. 7. Arrhenius plots of the ionic conductivity of $Ce_{1-x}Eu_xO_{2-\delta}$ solid solutions.

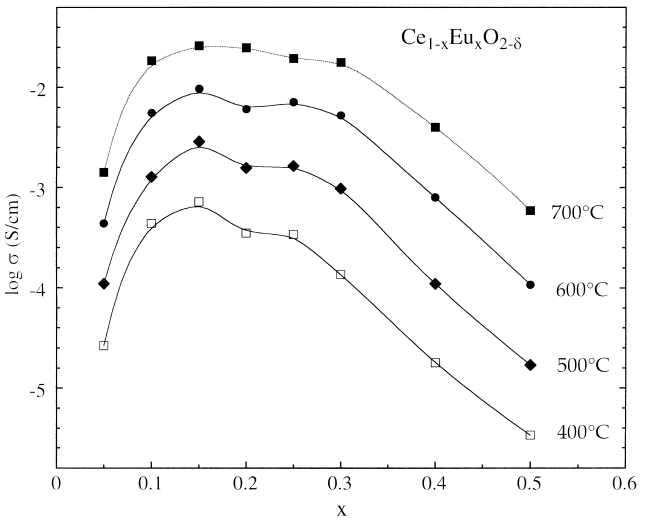


Fig. 8. Variation of the conductivities of $Ce_{1-x}Eu_xO_{2-\delta}$ solid solutions as a function of $x$ at temperatures 400, 500, 600 and 700°C.

states) with $Eu^{2+}$, $Eu^{3+}$ and mixed valent standards (inset) indicates unambiguously a $Eu^{3+}$ ($4f^6$) state in this material. The fact that the ''as prepared'' (LT, 260°C) material spectrum exhibits a sharper WL feature than the material that was annealed at 1300–1400°C (HT) should also be noted. This behavior could reflect a narrowing of the 5d final states due to more disorder in the local bonding in the LT synthesized material (relative to the structurally relaxed HT annealed materials).

The C feature in the $Ce_{1-x}Eu_xO_{2-\delta}$ spectrum (see Fig. 9) involves single and multiple backscattering (of the outgoing photoelectron) from the O-ligand shell and has sometimes been dubbed a continuum resonance. The energy of this C feature has been shown empirically to shift systematically with varying R–O first shell distance (R is a rare earth here) [25]. The relatively constant position of the C features of all of the compounds indicates that the Eu–O first shell distance is similar in all of these materials.

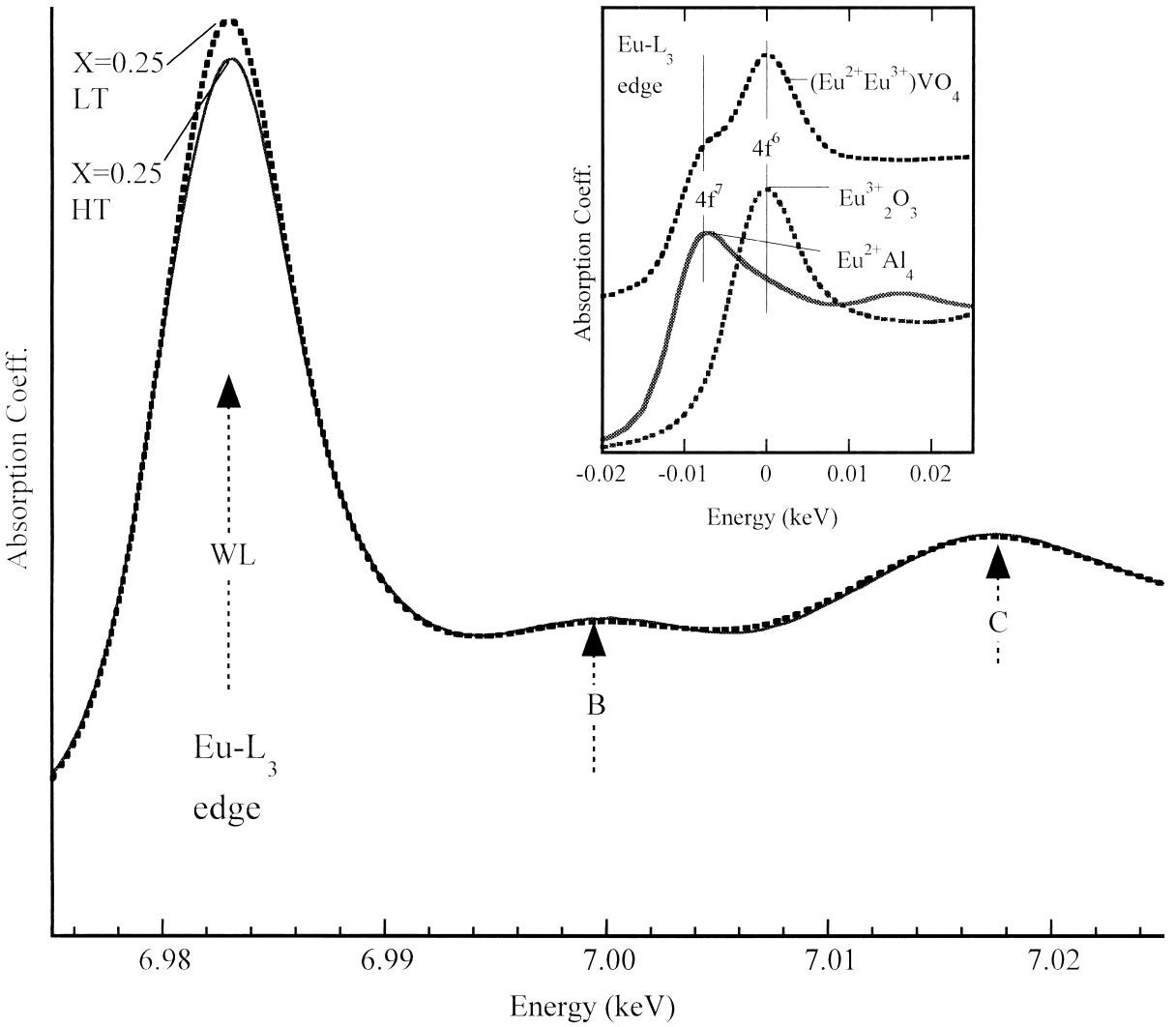


Fig. 9. Eu $L_3$-edges of $Ce_{0.75}Eu_{0.25}O_{2-\delta}$ ''as prepared'' (hydrothermally at 260°C, LT) and after a high temperature (HT) anneal (1300–1400°C). The inset compares the Eu $L_3$-edges of a $Eu^{3+}$ ($4f^6$), a $Eu^{2+}$ ($4f^7$), and a mixed valent Eu ($4f^6/4f^7$) standard compound (see Ref. [24]). Note the dramatic shift in the WL feature between the two Eu 4f states and the doubling of this feature in the mixed valent material. The weaker B and C features (in the main figure) are related to the distribution of near neighbors in the solid and are discussed in the text.

## 4. Conclusions

$Ce_{1-x}Eu_xO_{2-\delta}$ ($x = 0$–$0.25$) solid solutions with the fluorite structure were prepared for the first time by the soft hydrothermal method using $NH_4OH$ as mineralizer at 260°C and ~10 MPa. Ultrafine particles of uniform crystallite dimension ~40–55 nm can be formed in 1 h under hydrothermal conditions. Further heat treatment slowly increases the crystallinity of the powder from ~25 nm crystallite size in 30 min to ~35–55 nm in 12 h. Because of the small particle size of the ceria powder, the sintering temperature needed to obtain a dense ceramic pellet was reduced substantially from 1650–1700°C, that required for the ceria solid electrolytes prepared by conventional solid state methods, to ~1300°C. The highest conductivity found in $Ce_{0.85}Eu_{0.15}O_{1.925-\delta}$ ($\sigma_{700°C} = 2.6 \times 10^{-2}$ S/cm; $E_a = 0.66$ eV) is predominantly ionic and one to two orders of magnitude higher than that of the most commonly used solid electrolyte, stabilized zirconia ($\sigma_{700°C} < 10^{-3}$–$10^{-4}$ S/cm). The coefficients of thermal expansion, determined from high-temperature X-ray data, are $11.8 \times 10^{-6}$ $K^{-1}$ for $CeO_2$ and slowly increase with increasing Eu substitution ($14.0 \times 10^{-6}$ $K^{-1}$ at $x = 0.25$).

## References


[1] T. Takahashi, A. Kozawa (Eds.), Application of Solid Electrolytes, JEC Press, Cleveland, OH, 1980.
[2] T. Takahashi (Ed.), High Conductivity Solid Ionic Conductors, World Scientific, Singapore, 1989.
[3] W. Göpel, T.A. Jones, M. Kleitz, I. Lundström, T. Seiyama (Eds.), Chemical and Biochemical Sensors, Vols. 2 and 3, VCH, Weinheim, 1991/1992.
[4] T.H. Etsell, S.N. Flengas, Chem. Rev. 70 (1970) 339.
[5] B.C.H. Steele, Sci. Ceram. 10 (1980) 1.
[6] E. Subbarao, H.S. Maiti, Solid State Ionics 11 (1984) 317.
[7] B.C.H. Steele, J. Power Sources 49 (1994) 1.
[8] S.P.S. Badwal (Ed.), Science and Technology of Zirconia, Technomic, Lancaster, UK, 1993.
[9] T. Takahashi, H. Iwahara, Mater. Res. Bull. 13 (1978) 1447.
[10] A.M. Azad, S. Larose, S.A. Akbar, J. Mater. Sci. 29 (1994) 4135.
[11] P. Shuk, H.-D. Wiemhöfer, U. Guth, W. Göpel, M. Greenblatt, Solid State Ionics 89 (1996) 179.
[12] H. Inaba, H. Tagawa, Solid State Ionics 83 (1996) 1.
[13] A. Trovarelli, Catal. Rev. Sci. Eng. 38 (1996) 439.
[14] P.J. Gellings, H.J.-M. Bouwmeester, Catal. Today 1 (1992) 1.
[15] Y.C. Zhou, M.N. Rahaman, J. Mater. Res. 8 (1993) 1680.
[16] K. Yamashita, K.V. Ramanujachary, M. Greenblatt, Solid State Ionics 81 (1995) 53.
[17] W. Huang, P. Shuk, M. Greenblatt, Chem. Mater. 9 (1997) 2240.
[18] P.J. Gellings, H.J.-M. Bouwmeester (Eds.), The CRC Handbook of Solid State Electrochemistry, CRC Press, Boca Raton, FL, 1997.
[19] H.-H. Möbius, Extended Abstracts 37th Meeting ISE, Vilnius, USSR, 24–31 Aug. 1986, Vol. 1, p. 136.
[20] Y. Teraoka, H.M. Zhang, S. Furukawa, N. Yamazoe, N. Chem. Lett. N10 (1985) 1743.
[21] P. Shuk, M. Greenblatt, Solid State Ionics 116 (1999) 217.
[22] P. Shuk, M. Greenblatt, M. Croft, Chem. Mater. 11 (1999) 273.
[23] R.D. Shannon, C.T. Prewitt, Acta Crystallogr. 32A (1976) 751.
[24] K.V. Ramanujachary, J.E. Sunstrom, I. Fawcett, P. Shuk, M. Greenblatt, M. Croft, I. Novick, R.H. Herber, S. Khalid, Mater. Res. Bull. 34 (1999).
[25] Y. Jeon, F. Lu, H. Jhans, S. Shaheen, G. Liang, M. Croft, P. Ansari, K.V. Ramanujachary, E. Hayri, S. Fine, S. Li, X. Feng, M. Greenblatt, L. Green, J. Tarascon, Phys. Rev. B 36 (1987) 3891.